CHEMISTRY

Visible light–initiated radical 1,3-difunctionalization of β,γ-unsaturated ketones

Ruihua Liu[1], Yang Tian[1], Jie Wang[2], Zemin Wang[1], Xiangqian Li[1], Chenyang Zhao[2]†, Ruoyu Yao[1], Shuo Li[1], Leifeng Yuan[1], Jinbo Yang[2]*, Dayong Shi[1,3]*

Radical-mediated 1,2-difunctionalization of olefins is a well-established synthetic technique widely used in the rapid construction of structurally diverse molecular entities. However, radical-mediated 1,3-difunctionalization reactions are rare, and the substrates are generally limited to strained skeletons. Here, we report a practical approach for 1,3-difunctionalization of available β,γ-unsaturated ketones via a radical cascade process including visible light–irradiated radical addition, thermodynamic stability–driven 1,2-carbonyl migration from unactivated all-carbon quaternary center, and terminal C-radical varied transformations. Various highly functionalized alkyl skeletons with different valuable functional groups at positions 1 and 3 and the carbonyl group at position 2 have been synthesized through a radical chain pathway or Cu-catalyzed Ritter-type reaction. Moreover, this protocol provides a real case of diversity-oriented radical rearrangement for drug discovery. We identified a previously unknown chemotype of dual inhibitors for hypoxia-inducible factor (HIF) and WNT signaling pathways from products. These small-molecule inhibitors could suppress HIF and WNT signaling–dependent HCT116 cell growth in 2D and 3D culture systems.

INTRODUCTION

Emerging infectious diseases and the growing drug resistance of traditional diseases urge humans to accelerate the discovery of drugs to address these challenges. Chemists are committed to developing practical synthetic strategies to access structurally diverse small molecules for drug screening. Radical-mediated 1,2-difunctionalization of olefins has been persistently concerned by the organic synthetic community because of its usefulness in rapidly increasing molecular complexity and diversity (Fig. 1A) (*1*–*3*). However, radical-mediated 1,3-difunctionalization of unactivated substrates is rare and hard to be harnessed (*4*–*9*). In the past decades, radical-mediated strain release of strained ring systems has been regarded as a valid strategy for constructing 1,3-difunctionalized products. However, the substrates were generally limited to the structurally specific strained skeletons such as cyclopropanes (*4*), bicyclo[1.1.0]butanes (*5*), and [1.1.1]propellanes (Fig. 1A) (*6*, *7*). To expand the new chemistry space, we report a practical approach for 1,3-difunctionalization of readily accessible β,γ-unsaturated ketones via radical-mediated 1,2-carbonyl migration from the unactivated all-carbon quaternary center.

The altered localization of a carbonyl group on a molecular skeleton can profoundly influence the molecular biological and physical properties and potential synthetic applications (*10*, *11*). For example, the urea-thiophene carboxamide synthesized from the N-BOC 2-tropinone is a better active protective agent treating aminoglycoside-induced hearing loss than the C3 analog (*11*). Currently, carbonyl migrations triggered by transition metal–promoted C(C═O)—C σ-bond activation have been well explored, enabling multifarious synthetically and pharmaceutically valuable transformations (Fig. 1B) (*12*–*15*). Nevertheless, these reactions profoundly depend upon high temperature (*13*), and the substrates are generally limited to strained cyclic ketones (*14*) and directing group incorporated ketones (*15*) due to the inherent stability of C—C σ-bonds and the poor reactivity between the C—C σ-orbit and the transition metal center (*16*). Consequently, it is highly desirable to explore the site-selective carbonyl migration of readily available β,γ-unsaturated ketones under mild reaction conditions.

The carbonyl group is one of the most widely studied chromophores in photochemistry (*17*). Various excited-state carbonyl-mediated photochemical reactions have been extensively applied to synthetic chemistry (*18*–*21*). Among them, the light-initiated carbonyl migration of β,γ-unsaturated carbonyl compounds is a fascinating area in synthetic chemistry because of the presence of both alkene and carbonyl chromophores in a substrate (*19*). Previous studies reveal that two unique carbonyl migration pathways, including oxadi-π-methane (ODPM) rearrangement (*20*) and 1,3-carbonyl shift (*21*), exist in ultraviolet (UV) light–irradiated rearrangement reactions of β,γ-unsaturated ketones (Fig. 1C). The ODPM rearrangement proceeds from the ππ* excited state (T1) of the alkene moiety (*20*). In contrast, the 1,3-carbonyl migration generally originates from the nπ* excited state of the carbonyl group (Fig. 1C) (*21*). These reactions are useful; β,γ-unsaturated carbonyl compounds also undergo many complex competitive reactions known for isolated ketones or olefins simultaneously under UV light–irradiated conditions (*17*, *19*). These complex competitive reactions have challenged molecular skeletal selective modification considerably. Drawing inspiration from the advancements of visible light–irradiated radical reactions over the past few decades (*22*, *23*) and the conventional radical addition-driven functional group migration reactions (*24*–*26*), we designed and successfully developed a practical 1,3-difunctionalization of β,γ-unsaturated

[1]State Key Laboratory of Microbial Technology, Shandong University, 72 Binhai Road, Qingdao 266237, Shandong, P. R. China. [2]Key Laboratory of Marine Drugs, Ministry of Education of China, School of Medicine and Pharmacy, Ocean University of China, Qingdao 266003, Shandong, P. R. China. [3]Laboratory of Marine Drugs and Biological Products, Pilot National Laboratory for Marine Science and Technology, 168 Weihai Road, Qingdao 266237, Shandong, P. R. China.
†Present address: Department of Cancer Biology, Cleveland Clinic, 9500 Euclid Ave, Cleveland, OH 44195, USA.
*Corresponding author. Email: shidayong@sdu.edu.cn (D.S.); yangjb@ouc.edu.cn (J.Y.)

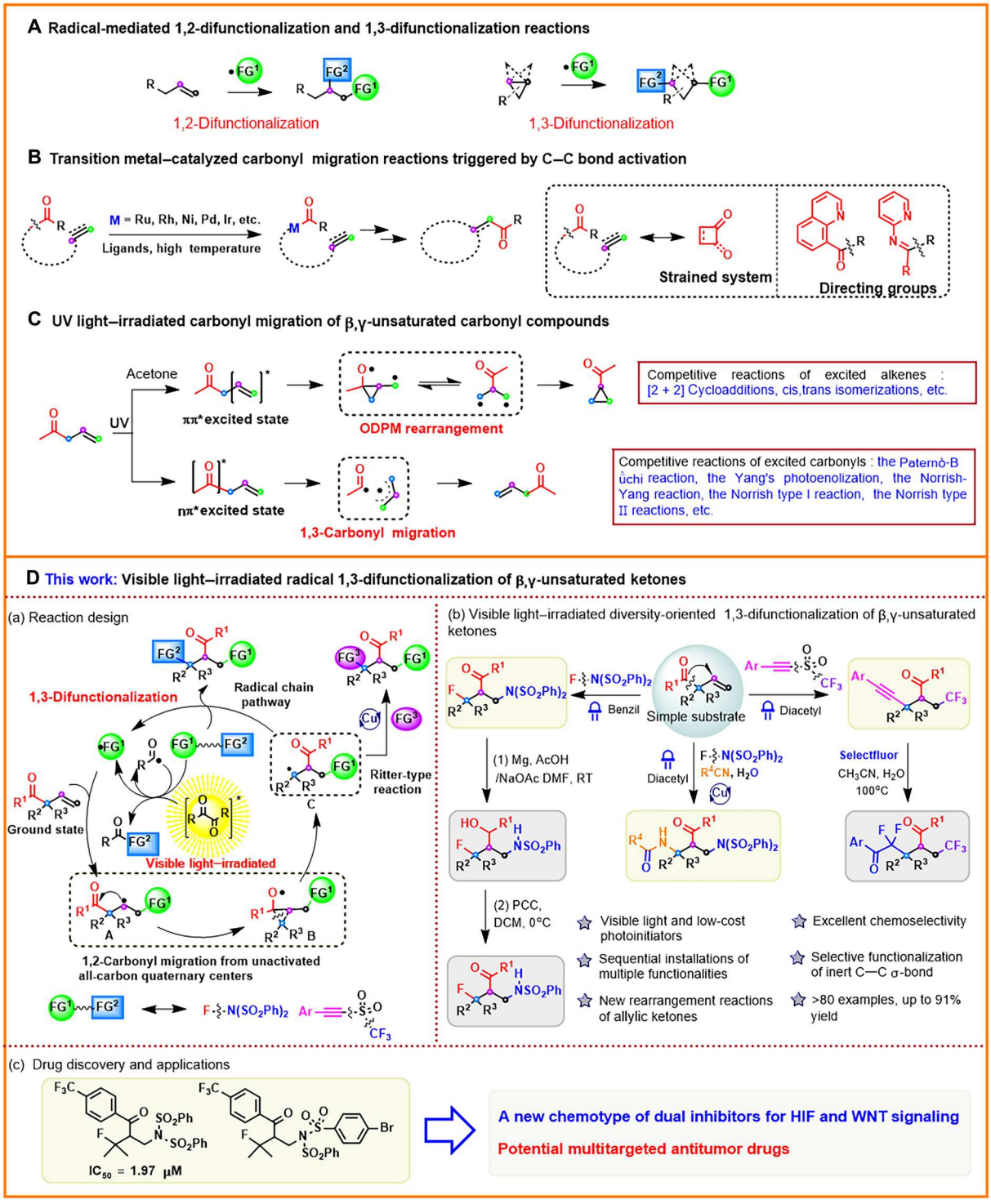

Fig. 1. Background and the present research. (**A**) Radical-mediated 1,2-difunctionalization and 1,3-difunctionalization reactions. (**B**) Transition metal–catalyzed carbonyl migration reactions triggered by C—C bond activation. (**C**) UV light–irradiated carbonyl migration of β,γ-unsaturated carbonyl compounds. (**D**) This work: Visible light–irradiated radical 1,3-difunctionalization of β,γ-unsaturated ketones.

ketones via a radical cascade process (Fig. 1D). The cascade process includes visible light–irradiated radical addition, thermodynamic stability–driven 1,2-carbonyl migration from unactivated all-carbon quaternary center, and terminal C-radical varied transformations (Fig. 1D, a). Unlike UV light–irradiated complex competitive reactions occurring from self-excited β,γ-unsaturated ketones (*19*), this visible light–mediated rearrangement reaction was initiated by the interaction between excited α-diketones and radical difunctional reagents [*N*-fluorobenzenesulfonimide (NFSI) or acetylenic triflones], producing the radical intermediate •FG[1] (Fig. 1D, a) (*27*). The •FG[1] then attacked the alkene moiety, giving the secondary C-radical intermediate **A**. The intermediate **A** underwent radical cyclization to form the alkoxy radical **B**. A more stable tertiary C-radical **C** was readily formed by C—C σ-bond selective scission. Last, the tertiary C-radical **C** was trapped by difunctional radical reagents, delivering the 1,2,3-trifunctionalized alkyl skeletons and regenerating the addition radical •FG[1] (*28*, *29*). The radical chain pathway could also be terminated through the Cu-catalyzed Ritter-type reaction, gaining the terminal radical ammoniation products (*30*). Various highly functionalized alkyl skeletons with different valuable functional groups at positions 1 and 3 and the carbonyl group at position 2 were obtained with excellent chemoselectivity and regioselectivity (Fig. 1D, b). This strategy may be helpful for drug discovery because it provides a practical pathway to rapidly construct structurally diverse and highly functionalized molecules from simple frameworks (Fig. 1D, c).

The hypoxia-inducible factor (HIF) pathway is a promising target for cancer therapeutics because it regulates many cellular adaptive biological processes like glucose metabolism and angiogenesis that help tumor cells survive and proliferate under hypoxic conditions (*31*–*33*). The WNT signaling pathway regulates fundamental cellular processes, including differentiation, proliferation, migration, and survival (*34*). Dysregulation of WNT signaling may lead to multiple human cancers, for example, breast cancer, colorectal cancer, melanoma, and so on (*35*). Moreover, these two pathways could both be aberrantly activated in the tumor microenvironments (*36*), in which mutation-driven WNT signaling (*37*) and hypoxia- or nutrient deprivation–induced HIF activities (*38*) could exist simultaneously. We compared the mRNA expression profiles of typical HIF signaling targeting genes (*Hif1α, Pgk1, Slc2a1, Tfrc, and Timp1*) and WNT signaling targeting genes (*Axin2, Cyclin D1, and β-Catenin*) using the online GEPIA2 web server (http://gepia2.cancer-pku.cn/#analysis) in different cancers and their paired normal tissues (*39*). The expression levels of both HIF and WNT signaling on tested downstream genes are notably higher in the tumor samples of cholangiocarcinoma (CHOL), colon adenocarcinoma (COAD), lymphoid neoplasm diffuse large B cell lymphoma (DLBC), esophageal carcinoma (ESCA), brain lower-grade glioma (LGG), pancreatic adenocarcinoma (PAAD), rectum adenocarcinoma (READ), sarcoma (SARC), stomach adenocarcinoma (STAD), and testicular germ cell tumors (TGCT), suggesting that HIF and WNT signaling are simultaneously activated in these cancers (fig. S1). In addition, HIF1α and β-catenin proteins were both detected positively (*40*) in the later stages of colorectal cancer (CRC). In all CRCs, more than 90% harbor a mutation that activates the canonical WNT signaling, and in archived CRC samples, 60% express high levels of the HIF1α protein (*41*). Moreover, the cross-talk between these two pathways has been reported (*42*). β-Catenin could form a complex with HIF1α and potentiate the expression of HIF1α classical target genes, thereby promoting cell survival during hypoxia (*43*). Inhibiting both β-catenin and HIF1α signaling will help to more efficiently diminish HIF1α function. On the other hand, HIF1α has a direct role in inhibiting β-catenin and reduced HIF-1α leads to increased β-catenin–dependent activation of T cell factor 4 (TCF-4) transcriptional activity (*37*, *38*), which is positively associated with tumor cell proliferation. Although some small-molecule inhibitors specific for HIF or WNT signaling exhibit sound antitumor activity, no corresponding anticancer candidates are clinically available yet (*31*–*39*). Because HIF and WNT are both substantial pathways that affect tumor cell proliferation (*31*–*35*), the development of previously unknown multifunctional small-molecule inhibitors for both HIF and WNT signaling might be able to create avenues for treating the related cancers. We found a previously unknown chemotype of dual inhibitor for HIF and WNT signaling from structurally diverse product molecules. Therefore, these structurally distinct small-molecule inhibitors are promising in developing previously unidentified multitargeted antitumor drugs. Notable advantages of this protocol include (i) the unconventional 1,3-difunctionalization of allyl substrates via radical-mediated 1,2-migration of carbon-based groups, (ii) inert C—C σ-bond selective cleavage and functionalization, and (iii) rapid constructions of structurally diverse molecules with excellent chemoselectivity and potential bioactivities.

RESULTS AND DISCUSSION

Reaction optimization

At the beginning of this study, we chose β,γ-unsaturated ketone **1a** with a *gem*-dimethyl at the α-position of the carbonyl as the model compound. NFSI was used as a nitrogen-centered radical precursor and radical fluorination reagent to screen the reaction conditions (Table 1) (*28*). When cheap benzil was applied as a photoinitiator (**PI1**) (*27*), the designed reaction proceeded smoothly and gave the 1,3-difunctionalized product **3a** in a 59% yield irradiated with blue light-emitting diode (LED) for 30 hours under the argon atmosphere (Table 1, entry 1). Several photoinitiators, such as **PI2** to **PI5** (Table 1, entries 2 to 5), were tested but gave **3a** in unsatisfactory yields. Benzophenone (**PI6**) could not trigger this transformation under the same condition (Table 1, entry 6). Besides acetone, CH_3CN was an efficient solvent for this transformation by screening several solvents (Table 1, entries 7 to 11). However, only 3% of **3a** was obtained using toluene as the solvent (Table 1, entry 10). It is presumed that the intermolecular hydrogen abstraction reaction between the bissulfonamidyl radical and toluene suppressed the addition reaction between the bissulfonamidyl radical and the β,γ-unsaturated ketones. To enhance the yield of **3a**, the loading level of the photoinitiator was also evaluated (Table 1, entries 12 to 14). The yield could rise to 82% using 0.5 equiv of **PI1** (Table 1, entry 13). Control experiments revealed that **PI** and light were both essential for this transformation (Table 1, entries 15 and 16).

Investigation of the substrate scope

With the optimum conditions established (Table 1, entry 13), we investigated the substrate and reaction scope of this strategy (Fig. 2). This protocol proved to work for β,γ-unsaturated ketones bearing 4-substituted aryl rings with different electronic properties, delivering the products **3b** to **3g** in moderate to good yields. The β,

Table 1. Optimization of the reaction conditions.

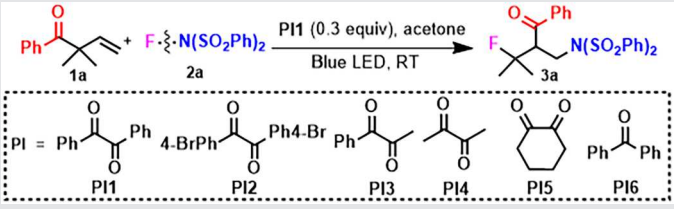

Entry	Variation of conditions*	3a (%)†
1	None	59
2	**PI2** instead of **PI1**	21
3	**PI3** instead of **PI1**	50
4	**PI4** instead of **PI1**	52
5	**PI5** instead of **PI1**	11
6	**PI6** instead of **PI1**	0
7	Acetonitrile instead of acetone	51
8	1,2-Dichloroethane instead of acetone	34
9	Dichloromethane instead of acetone	31
10	Toluene instead of acetone	3
11	*N,N*-dimethylformamide instead of acetone	25
12	**PI1** (0.4 equiv)	75
13	**PI1 (0.5 equiv)**	**82**
14	**PI1** (0.6 equiv)	81
15	No light	0
16	No **PI**	0

*Conditions: **1a** (0.1 mmol), **2a** (0.25 mmol), and **PI** (0.03 mmol) in acetone (0.3 ml) were reacted under Ar at room temperature for 30 hours under the irradiation of 6-W blue LED. †Isolated yield.

γ-unsaturated ketones bearing 2-substituted, 3-substituted, and polysubstituted aryl rings were all viable in this strategy, obtaining the corresponding 1,3-aminofluorination products (**3h** to **3p**) in good yields. Unexpectedly, the 1,2-carbonyl migration/cyclic byproducts **3i′** and **3o′** were formed using 2-bromophenyl or 2,4-dimethylphenyl substituted β,γ-unsaturated ketones as substrates. This transformation might be that the stereo-hindrance effect of ortho-substituents makes the generated tertiary C-radical center close to the aryl rings, facilitating the intramolecular cyclization reaction. Pyridine and thiophene incorporated β,γ-unsaturated ketones were also tolerated (**3q** and **3r**). Notably, the β,γ-unsaturated ketones synthesized from natural products, including L-(−)-menthol and D-fructopyranose, participated nicely in this strategy (**3s** and **3t**). This protocol tolerated the β,γ-unsaturated ketones bearing straight-chain or branch-chain alkyl moieties well (**3u** to **3y**). Satisfying yields were obtained using unstrained and strained cyclic alkyl-substituted β,γ-unsaturated ketones (**3z** and **3aa**). Furthermore, alkyl-substituted β,γ-unsaturated ketones derived from complex natural products such as hydroxycitronellal and lithocholic underwent this transformation successfully (**3ab** and **3ac**). The reaction proceeded readily when the *gem*-dimethyl at the α-position of the carbonyl group was substituted by symmetric *gem*-diethyl (**3ad**), *gem*-dipropyl (**3ae**), cyclopentyl (**3af**), cyclohexyl (**3ag** and **3ah**), medium-sized cycloalkyl (**3ai** and **3aj**), *gem*-diphenyl (**3ak**), nonasymmetric *gem*-phenylmethyl (**3al**), *gem*-propylmethyl (**3am**), or *gem*-cyclopentylmethyl (**3an**). In addition, β,γ-unsaturated cyclohexanone and cyclododecylketone were used as substrates, forming the ring-expansion products (**3ao** and **3ap**) in moderate yields with high diastereoselectivity. The unsymmetrical NFSI was also a suitable partner for this transformation, leading to a good yield of **3aq**. Could transition metal terminate the product-forming radical chain process to achieve the diversified reconstruction of the quaternary carbon center? The visible light–driven Cu-catalyzed Ritter-type reaction of β,γ-unsaturated ketones with nitriles was successfully developed (Fig. 3 and table S3) (*30*). This strategy proceeded smoothly using various straight-chain/branch-chain alkyl nitriles and benzonitrile (**4a** to **4e**). Various β,γ-unsaturated aryl ketones were also compatible in this visible light–driven metal-catalyzed radical cascade process (**4f** to **4l**).

Various acetylenic triflones were subjected to react with β,γ-unsaturated ketones under similar conditions to document the generality of this radical chain process (Fig. 4 and table S4) (*29*). Notably, arylacetylene-derived acetylenic triflones with different functional groups, including Cl, Br, CF_3, Et, Ph, and F, at the aryl moiety were all well tolerated, gaining 1,3-alkynyltrifluoromethylation products **6a** to **6g** in moderate to good yields using 0.6 equiv of diacetyl as the photosensitizer. Thiophene- and naphthalene-incorporated acetylenic triflones were compatible in this reaction, building the 1,3-alkynyltrifluoromethylation products **6h** and **6i** in moderate yields. The cascade processes involving a variety of β,γ-unsaturated aryl ketones were also successful, as demonstrated by the moderate yields of products (**6j** to **6x**). However, the alkyl-substituted β,γ-unsaturated ketones were less effective for this reaction, obtaining the mixture of carbonyl migrated products (**6y** and **6z**) and the alkene difunctionalized products (**6y′** and **6z′**) (*29*). In addition, the alkenyl triflone was not a suitable difunctional reagent for this strategy, and almost all of the β,γ-unsaturated ketone and alkenyl triflone were recovered (fig. S8).

The feasibility of radical-mediated remote carbonyl migration was also examined. Unfortunately, no carbonyl migration products were found using the distal unsaturated ketone **7** and only forming the alkene difunctionalized product **9′** in a 52% yield (Fig. 5A) (*30*). The practicability of this protocol was proven by performing gram-scale reactions (Fig. 5B). The follow-up transformations of the products were ultimately performed to examine the synthetic potentiality and utility of these reactions. The reduction leads to the desulfonylated alkyl alcohol **10** by treating **3a** with magnesium powder in a mixed solution of *N,N′*-dimethylformamide and buffer (Fig. 5B, a). The desulfonylated ketone **11** was also readily obtained through pyridinium chlorochromate–mediated oxidation of the corresponding alkyl alcohol (Fig. 5B, b). Selectfluor readily oxidized the alkynyl moiety on product **6a** to construct the desired 1-trifluoromethyl, 3-difluoroalkyl ketone **12** in a 63% yield (Fig. 5B, c).

Mechanistic investigations

We conducted mechanistic experiments to elucidate the reaction details (Fig. 6). The reactions were entirely suppressed by 2,2,6,6-tetramethyl-1-piperidinyloxy (TEMPO) under standard conditions, and no products were formed (Fig. 6A). These results indicate

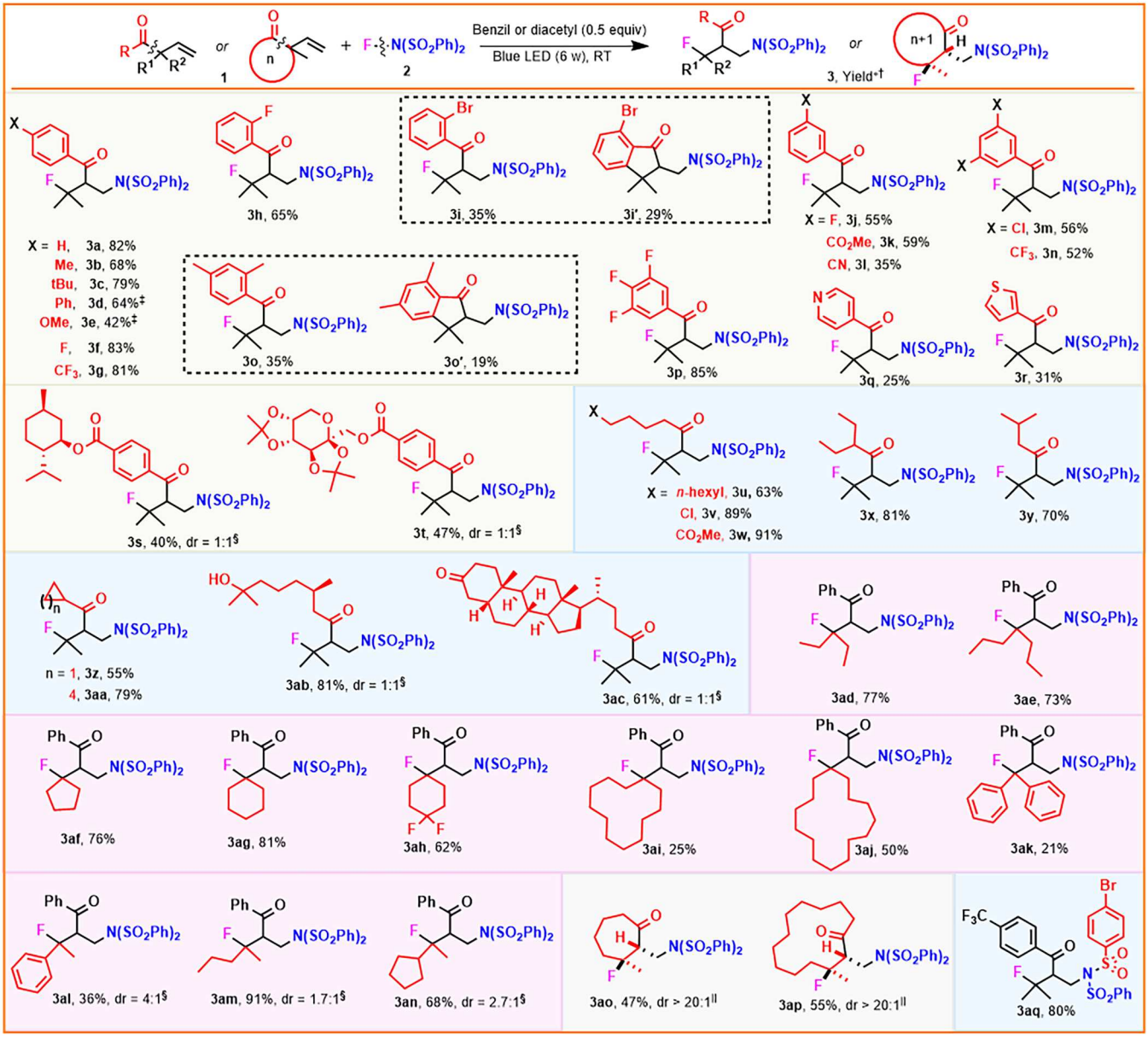

Fig. 2. 1,3-Aminofluorination of β,γ-unsaturated ketones. *Isolated yields. †Condition 1: **1** (0.1 mmol), **2a** (0.25 mmol), and benzil (0.05 mmol) were stirred in acetone (0.3 ml) and irradiated with 6-W blue LED under Ar at room temperature (RT) for 30 hours. ‡Diacetyl (0.05 mmol) was used instead of benzil. §The diastereoisomeric ratios were identified with ^{1}H NMR. ||The configuration of the diastereomer was confirmed by nuclear Overhauser effect.

that a radical process could be involved in this strategy. Both 1,3-carbonyl shift product **13** and ODPM rearrangement product **14** were not detected when subjecting β,γ-unsaturated ketone **1a** and α-diketones to the two standard conditions (Fig. 6B, a and b) (*19*, *20*, *21*). These results suggest that the reaction could not be initiated by direct irradiation of β,γ-unsaturated ketones or the interaction between the photoexcited α-diketones and β,γ-unsaturated ketones. Benzoyl fluoride **15** and the benzil dimerization product **16** were observed under the standard condition (Fig. 6B, c), giving vital clues to the radical initiation process. Previous studies and literature revealed that two possible pathways exist in the generation of benzoyl fluoride **15** (Fig. 6C) (*40*, *41*). One process is the light-mediated direct α-cleavage of α-diketones (Norrish I) (path a) (*40*). The formed acyl radical **D** reacts smoothly with NFSI to produce the N-radical intermediate **E** to initiate the reaction and generate acyl fluoride (*41*). The other is the excited-state α-diketones **F** interacting with NFSI to produce N-radical intermediate **E** to initiate the reaction and construct alkoxy radical intermediate **G** (path b) (*27*). The latter was converted into acyl radical **D** and acyl fluoride. The acyl radical **D** reacted smoothly with NFSI to initiate the reaction via path a. Crossover experiments were carried out to differentiate between these two potential radical initiation processes, as depicted in Fig. 6D (*42*). The crossover product **PI3** was not detected by irradiating the mixture of **PI1** and **PI4** with a blue LED

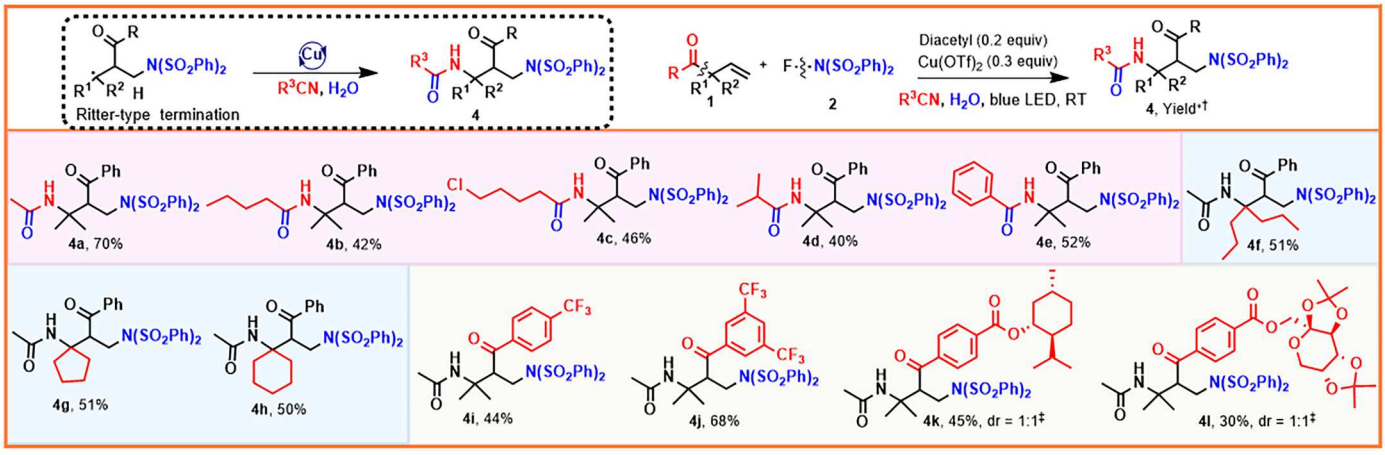

Fig. 3. 1,3-Diamination of β,γ-unsaturated ketones. *Isolated yields. †Condition 2: **1** (0.1 mmol), **2a** (0.25 mmol), diacetyl (0.02 mmol), and $Cu(OTf)_2$ (0.03 mmol) were stirred in various nitriles (1.0 ml) and H_2O (5.0 μl) and irradiated with blue LED under Ar at room temperature for 30 hours. ‡The diastereoisomeric ratios were identified with ^1H NMR or ^{13}C NMR.

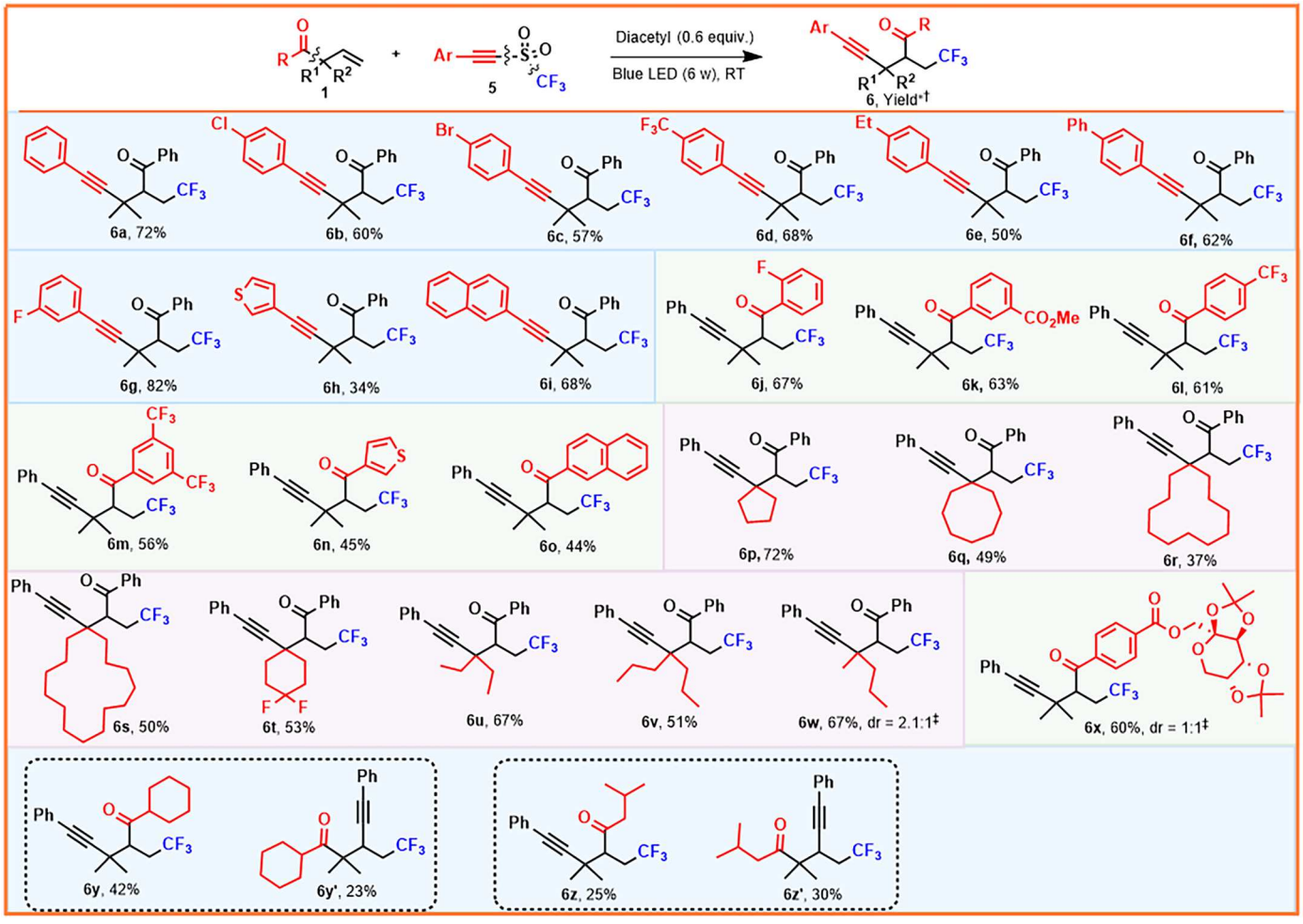

Fig. 4. 1,3-Alkynyltrifluoromethylation of β,γ-unsaturated ketones. *Isolated yields. †Condition 3: **1** (0.1 mmol), **2a** (0.25 mmol), and diacetyl (0.06 mmol) were stirred in acetone (0.3 ml) and irradiated with 6-W blue LED under Ar at room temperature for 30 hours. ‡The diastereoisomeric ratios were identified with ^1H NMR.

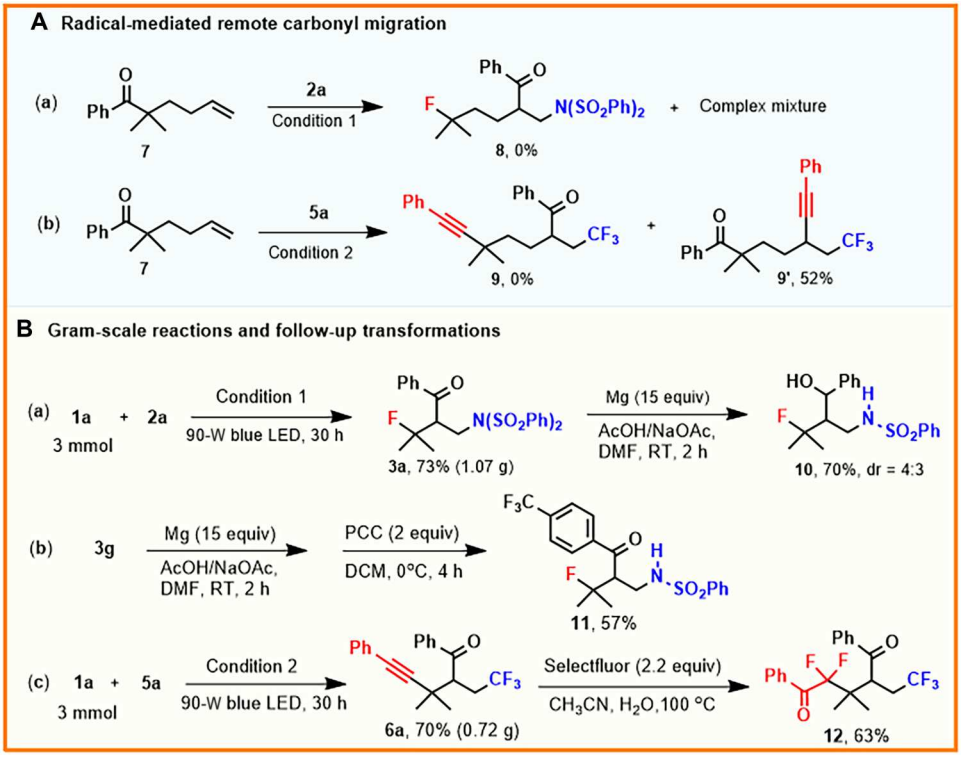

Fig. 5. Synthetic applications. (**A**) Radical-mediated remote carbonyl migration. (**B**) Gram-scale reactions and follow-up transformations.

for 48 hours. **PI1** and **PI4** were not detected using **PI3** as the substrate in the same way. While this result did not provide solid evidence for identifying the accurate radical initiation processes, it at least revealed that the light-mediated direct cleavage of α-diketones (Fig. 6C, path a) was probably not the radical initiation process, and path b was a more sensible alternative pathway. UV-visible (UV-vis) absorption spectrum verified that benzil is an effective photosensitizer for this reaction (Fig. 6E). "Light/dark" experiments were then conducted. A minor amount of 1,3-difunctionalized product was still detected after removing the light source (Fig. 6F). These results reveal that the product-forming radical chain process was involved in this reaction (*27*). Nonetheless, these reactions still need continuous irradiation due to the short lifetimes of radical chain processes.

Bioactivity studies

We constructed the corresponding luciferase reporter systems to identify previously unidentified compounds that can effectively inhibit HIF and WNT signaling pathways for related cancer treatment (fig. S15A). HIF and WNT signaling pathways are both activated in HCT116 cells. β-Catenin is aberrantly activated in HCT116 cells owing to a 3–base pair deletion that removes one amino acid (Ser^{45}) (*43*), which blocks β-catenin degradation. Moreover, the HCT116 cell line expresses detectable HIF1α proteins under normoxia condition (*44*, *45*). In the tumor microenvironment, tumor cells face intrinsic elevated HIF and WNT activities due to mutations and encounter other cells and mediators, which will further enhance HIF/WNT activities. Because HCT116 cells have detectable levels of HIF and WNT under a steady state and also respond to additional stimulus treatment, this allows us to study all interested characteristics in the same cell under both resting and stimulatory states. Although no anticancer HIF and WNT inhibitors are clinically available, some small-molecule inhibitors specific for HIF (*46*) or WNT (*47*) signaling exhibit sound HCT116 cell growth inhibition activity. Therefore, HIF1α and WNT luciferase reporter systems were developed in the HCT116 cells through multiple steps, which resulted in generating constructs that consisted of the luciferase reporter gene under the transcriptional regulation of an enhancer containing hypoxia-responsive element (HRE) or β-catenin–binding cis element (TCF/LEF1) upstream of a mini-TATA promoter, respectively. Upon the binding of HIF1α protein to HRE or the binding of β-catenin to TCF/LEF1, the luciferase reporter gene is transcriptionally activated. The luciferase expression level represents the DNA binding efficiency of HIF1α or β-catenin, which depends on their function and the expression levels. Decreased luciferase activity reflects the inhibitory effects of tested compounds on the corresponding signaling. The established drug screening workflow screened nearly 20,000 small molecules (*48*). Several 1,3-aminofluorination and 1,3-diamination products, as shown in Figs. 2 and 3, were identified to have the capacity to inhibit both WNT and HIF signaling activities (Fig. 7, A and B). Among them, the two most potent compounds were **3g** and **3aq**, which had an inhibition rate of 59.7 and 66.2% for WNT signaling and 50.2 and 68.4% for HIF signaling, respectively, while LF3 and KC7F2 (*49*), which are known to inhibit WNT and HIF activity, showed 55 and 53% inhibition activity at 5 μM in our reporter systems. The bissulfonamidyl ($N(SO_2Ph)_2$) group is an essential moiety because of the poor inhibitory effects of the desulfonylated product **11.** Considering the representativeness and the effectiveness, **3g** was subjected to further investigation. Whether **3g** had

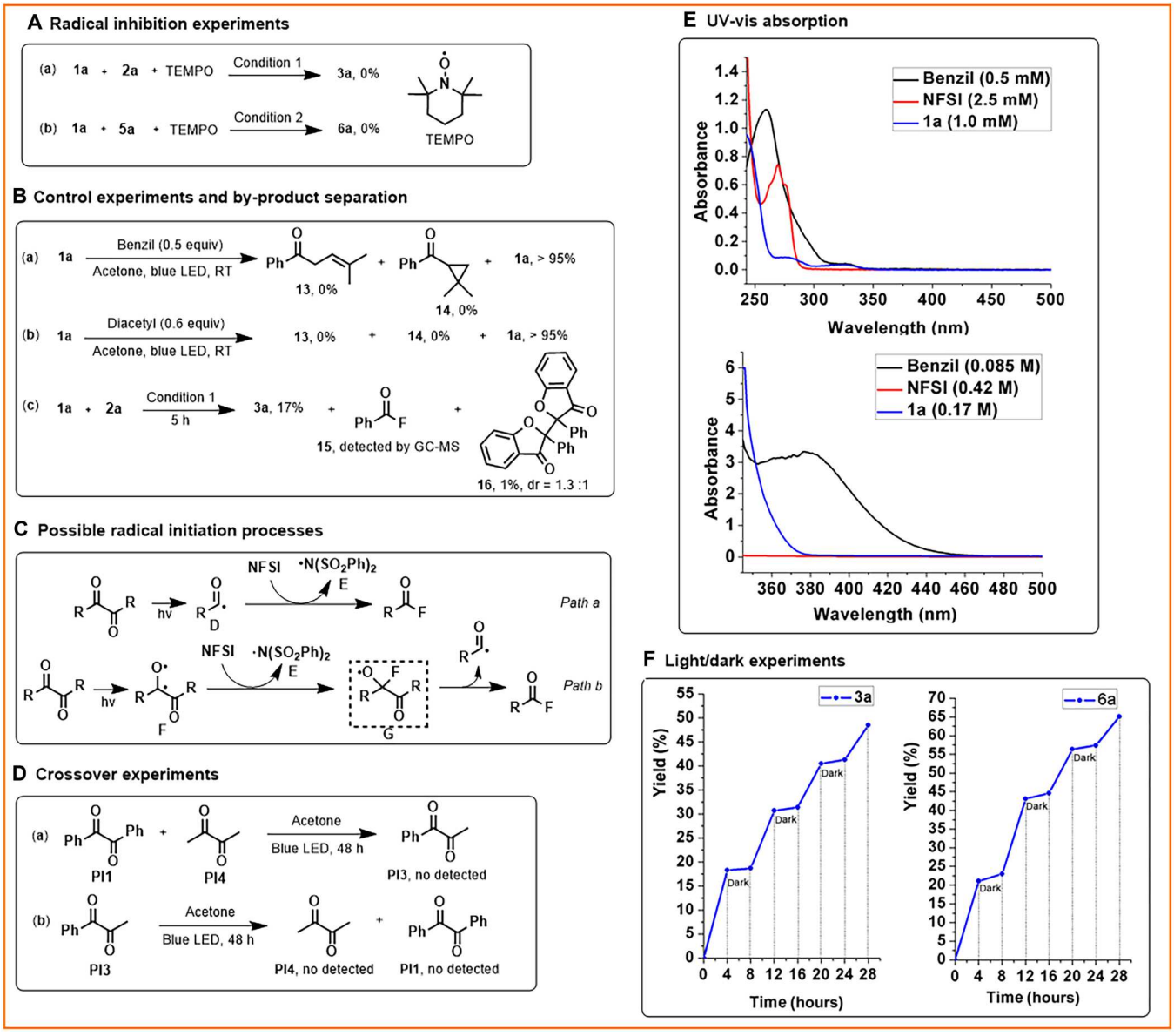

Fig. 6. Mechanistic experiments. (**A**) Radical inhibition experiments. (**B**) Control experiments and by-product separation. (**C**) Possible radical initiation processes. (**D**) Crossover experiments. (**E**) UV-vis absorption. (**F**) Light/dark experiments.

inhibitory effects on P53, signal transducer and activator of transcription (STAT)–nuclear factor κB (NFκB), and peroxisome proliferator–activated receptor (PPAR) signaling pathways, which are closely associated with cancer, was also detected. The results showed that **3g** exhibited trivial or much less inhibition toward these pathways compared with its inhibitory efforts on HIF and WNT signaling pathways, which implied the efficacy and specificity of **3g** to inhibit HIF and WNT signaling (fig. S15B). From the PhyChem predictions (*50*), **3g** obeys most parameters of the Lipinski rule of five: Log*P* = 3.4 (<5), hydrogen bond acceptors = 6 (<10), and hydrogen bond donors = 0 (<5) and shows drug-like properties. Because **3g** could potently inhibit HIF signaling, we first examined whether HIF protein expression was altered by **3g** treatment under both normoxia and $CoCl_2$-induced hypoxia (*51*). As shown in Fig. 7 (C and D), both HIF1α and HIF2α protein levels were inhibited by **3g** in a dose-dependent manner regardless of the culture conditions. Consistent with these results, the mRNA levels of typical HIF target genes *Bnip3* (Fig. 7E) and *Pgk1* (fig. S16D) were notably reduced by **3g** treatment. HIF1β protein levels were not influenced by **3g** treatment, indicating that **3g** might inhibit HIF signaling by modulating HIFα protein accumulation (Fig. 7, C and D). To further illustrate the possible mechanisms of **3g** inhibitory effect on HIFα protein accumulation, we examined whether the decreased HIFα proteins′ expression induced by **3g** was regulated at the protein synthesis step. To address this question, MG132, a proteasome inhibitor, was added to cell culture medium to block protein degradation by the proteasome (*52*), which allowed us to look at the **3g** effect on protein synthesis activities without the influence of the protein degradation

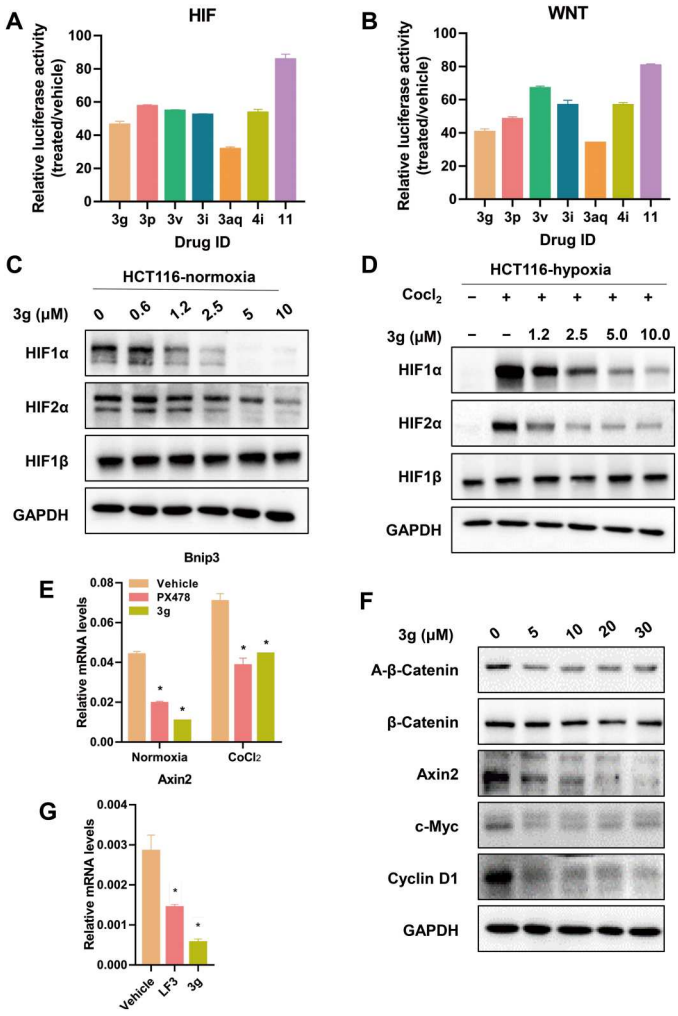

Fig. 7. 3g is identified as a dual inhibitor for HIF and WNT signaling pathways. Ten thousand HCT116-HRE-luci (**A**) or HCT116-TCF-luci (**B**) cells were seeded into each well of a 96-well plate. After overnight culture, cells were treated with the indicated compounds (10 μM) for 24 hours, and then luciferase activities were determined. HCT116 cells were cultured under either normoxia (**C**) or hypoxia (100 μM $CoCl_2$) (**D**) with vehicle or **3g** at the indicated concentrations for 24 hours. Whole-cell lysates were extracted for Western blot. GAPDH serves as the loading control. (**E**) HCT116 cells were treated with **3g** (10 μM) or PX478 (20 μM) for 24 hours in the presence or absence of $CoCl_2$. The mRNA level of HIF target gene *Bnip3* was determined by real-time polymerase chain reaction (RT-PCR) and normalized to *β-actin*. (**F**) HCT116 cells were treated with **3g** for 24 hours, and then the cell lysate was analyzed by Western blot. (**G**) HCT116 cells were treated with **3g** (10 μM) or LF3 (20 μM) for 24 hours. Expression level of β-catenin target gene *Axin2* was quantified by RT-PCR and normalized to *β-actin*. The individual experiments were repeated at least three times. Error bars indicate means ± SD. *$P < 0.05$ was considered statistically significant (treated versus vehicle), two-way ANOVA for (F) and one-way ANOVA for (G).

process. As shown in fig. S16A, both HIF1α and HIF2α proteins were accumulated upon MG132 treatment, and **3g** markedly suppressed the accumulation of HIFα proteins, whereas the HIF1β protein level was left unaffected, suggesting that **3g** can inhibit HIFα proteins' accumulation by reducing protein translational synthesis. Consistently, the phosphorylation of eIF4E, which controls the protein translation initiation (*53*), was strongly suppressed by **3g** (fig. S16, B and C). These results suggested that **3g** is an effective inhibitor of HIF signaling mainly by inhibiting the HIFα protein synthesis. Similarly, **3g** inhibition efficiency on WNT signaling was also determined. It was shown that **3g** could inhibit both active β-catenin and the expression of WNT target genes *Axin2*, *c-Myc*, and *CyclinD1* in a dose-dependent manner (Fig. 7F). Consistently, the mRNA abundance of typical WNT target genes *Axin2* (Fig. 7G) and *CyclinD1* (fig. S15C) was notably suppressed by **3g.** In conclusion, the data suggested that **3g** could function as a dual inhibitor for HIF and WNT signaling pathways.

Next, we evaluated the efficacy of **3g** in inhibiting these two pathways. Both HIF and active β-catenin driving luciferase activities were determined. They were inhibited by 24-hour **3g** treatment with an EC_{50} (median effective concentration) value of 11.37 μM (Fig. 8A) and 9.17 μM (Fig. 8B) for HIF and WNT signaling, respectively. Because HIF and WNT are significant pathways that affect

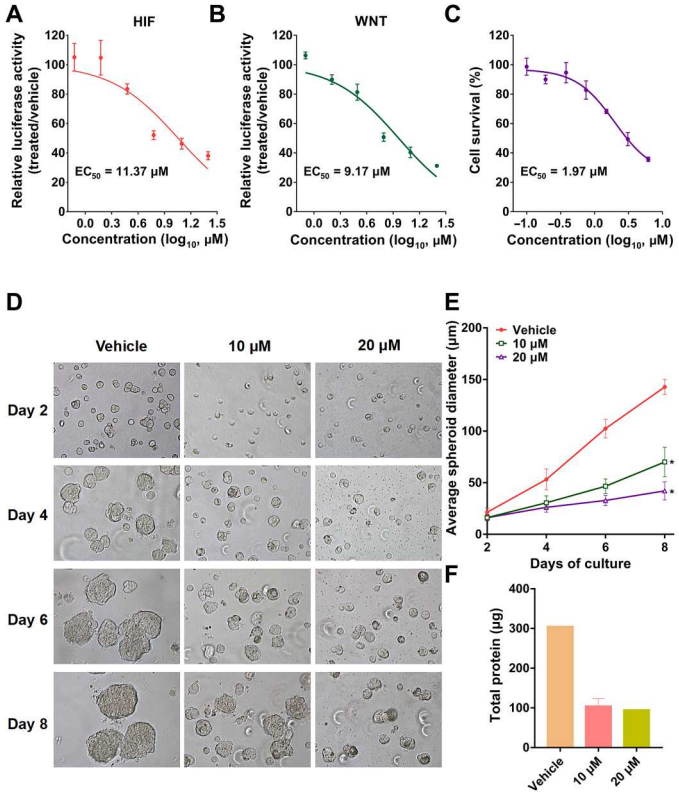

Fig. 8. 3g inhibits HIF and WNT signaling–dependent HCT116 cell growth in 2D and 3D culture systems. Ten thousand HCT116-HRE-luci (**A**) or HCT116-TCF-luci (**B**) cells were seeded into each well of a 96-well plate. After culturing overnight, cells were then treated with **3g** and luciferase activities were determined after 24 hours. (**C**) HCT116 cells (3000 per well) were plated into 96-well plates and cultured overnight. **3g** at various concentrations was added for an additional 72 hours, and cell viability was determined. (**D**) HCT116 cells (80,000 per well) were plated in a 24-well plate and cultured for 8 days with or without **3g** treatment, and the medium was changed every 2 days. Spheroids were observed using a microscope with ×20 magnification at days 2, 4, 6, and 8. At the end, total cell protein was extracted and quantified. (**E** and **F**) The spherical diameter was analyzed by Photoshop, and the quantification was performed by ImageJ software. The individual experiments were repeated at least three times. Error bars indicate means ± SD. *$P < 0.05$ was considered statistically substantial (treated versus vehicle using two-way ANOVA).

tumor cell proliferation (*54*), **3g** is likely to inhibit WNT and HIF signaling–addicted tumor cell growth. Therefore, HCT116 cells were used to measure the **3g** effects on cell viability because of its aberrant activation of the WNT signaling pathway due to the β-catenin mutation (*43*) and the high expression of HIF proteins (*44*, *45*). The results showed that **3g** could notably suppress HCT116 cell survival with an IC_{50} (median inhibitory concentration) at 1.97 μM in normoxia (Fig. 8C). The data indicated that **3g** as a dual HIF and WNT signaling inhibitor could inhibit HCT116 cell growth in a dose-dependent manner. Although two-dimensional (2D) culture is a well-known drug evaluation system, recent studies suggest that it lacks the cell-cell and cell–extracellular matrix signals in in vivo circumstances (*55*). 3D culture systems are emerging and believed to better simulate tumor characteristics in vivo. Moreover, the spheroids formed in 3D culture have a limited oxygen concentration at their core (*55*). HIFs have been postulated to be the primary mediators of hypoxic responses, and 3D culture also has been suggested to be a perfect model to study the effects of HIF-specific compounds on tumor growth in vitro (*56*). Therefore, we evaluated **3g** antitumor effects in 3D cultured HCT116 cells. The growth of formed spheroids was reduced with **3g** treatment in a dose-dependent manner (Fig. 8D). After 8 days of culture, the average spheroid diameters in **3g**-treated groups were 70 μm (10 μM) and 42 μm (20 μM), respectively, compared with about 142.7 μm in the vehicle-treated group (Fig. 8E). The quantification of spheroids′ total proteins also suggested that **3g** inhibited HCT116 cell growth (Fig. 8F). The data suggested that **3g** could effectively suppress HIF and WNT signaling–dependent HCT116 cell growth in 2D and 3D culture systems.

In summary, a previously unknown visible light–irradiated diverse-oriented radical 1,3-difunctionalization of β,γ-unsaturated ketones has been successfully developed via radical-mediated 1,2-carbonyl migration from an unactivated all-carbon quaternary center. The 1,2-carbonyl migration without additional substituents and the selective functionalization of inert C—C σ-bonds have been readily implemented through radical chain pathway or Cu-catalyzed Ritter-type reaction. This protocol features high atom economy and practicability since exploiting the easily accessible NFSI or acetylenic triflones as both the additional radical precursors and carbon radical trapping reagents. This strategy discloses a previously unknown site-selective photochemical rearrangement reaction of β,γ-unsaturated ketones, which makes possible the direct and efficient synthesis of highly functionalized alkyl skeletons with different valuable functional groups at positions 1 and 3 and the carbonyl group at position 2. In addition, we found a previously unknown chemotype of dual inhibitors for HIF and WNT signaling from structurally diverse product molecules. These skeletal-distinct small-molecule inhibitors are promising in treating related cancers. Therefore, this work provides a vivid case of diversity-oriented radical rearrangement reaction for drug discovery (*57*). We expect that this work will inspire endeavors to explore diversity-originated radical rearrangement reactions.

MATERIALS AND METHODS

Chemical part

All reagents were obtained from commercial suppliers and used without further purification. Flash column chromatography was implemented using Tsingdao silica gel (200 to 300 mesh). ^{1}H, ^{13}C, and ^{19}F nuclear magnetic resonance (NMR) spectra were recorded with Bruker AVANCE NEO (600 and 400 MHz) spectrometers and Agilent DD2 600 (600 MHz). All chemical shifts were reported relative to tetramethylsilane [0 parts per million (ppm) for ^{1}H] and $CDCl_3$ (77.0 ppm for ^{13}C). Fourier transform mass spectra were measured with a Thermo Fisher Scientific Q-Exactive instrument, and accurate masses were reported for the molecular ion ($[M]^+$ or $[M]^-$). UV-vis data were measured on a UV-3600 UV-vis/near-infrared (NIR) spectrophotometer.

General experimental procedure for 1,3-aminofluorination of β,γ-unsaturated ketones

β,γ-Unsaturated ketones **1** (0.1 mmol), benzil (0.5 equiv, 0.05 mmol), NFSI (2.5 equiv, 0.25 mmol), and acetone (0.3 ml) were added to a 5-ml glass tube. The mixture was irradiated with blue LEDs under Ar for 30 hours at room temperature. The reaction solution was concentrated under vacuum. Purification by column chromatography on silica gel (EtOAc:petroleum ether = 1:20 to 1:1) afforded the desired products **3**.

General experimental procedure for 1,3-diamination of β,γ-unsaturated ketones

β,γ-Unsaturated ketones **1** (0.1 mmol), diacetyl (0.2 equiv, 0.02 mmol), $Cu(OTf)_2$ (0.3 equiv, 0.03 mmol), NFSI (2.5 equiv, 0.25 mmol), nitriles (1.0 ml), and H_2O (5 μl) were added to a 5-ml glass tube. The reaction solution was irradiated with blue LEDs under Ar for 10 hours at room temperature. The mixture was concentrated under vacuum. Purification by column chromatography on silica gel (EtOAc:petroleum ether = 1:20 to 1:1) afforded the desired products **4**.

General experimental procedure for 1,3-alkynyltrifluoromethylation of β,γ-unsaturated ketones

β,γ-Unsaturated ketones **1** (0.1 mmol), acetylenic triflones (2.5 equiv, 0.25 mmol), acetone (0.3 ml), and diacetyl (0.6 equiv, 0.06 mmol) were added to a 5-ml glass tube. The reaction solution was irradiated with blue LEDs under Ar for 30 hours at room temperature. The mixture was concentrated under vacuum. Purification by column chromatography on silica gel (EtOAc:petroleum ether = 1:100 to 1:20) afforded the desired products **6**.

Biological part

Antibodies and reagents

All antibodies were commercially available. The primary antibodies HIF-1α (D1S7W), HIF-2α (D6T8V), HIF-1β/ARNT (D28F3), eIF4E (C46H6), phospho-eIF4E (Ser^{209}), nonphospho (active) β-catenin ($Ser^{33/37}/Thr^{41}$) (D13A1), β-catenin (D10A8), Cyclin D1 (92G2), c-Myc (D3N8F), and Axin2 (76G6) were obtained from Cell Signaling Technology. Antibodies against glyceraldehyde-3-phosphate dehydrogenase (GAPDH) and α-tubulin (B-7) were from Santa Cruz Biotechnology and K. Chen, respectively. Protease inhibitor (catalog no. 11836145001) and phosphatase inhibitor cocktail (catalog no. 4906837001) tablets were bought from Roche Diagnostics, while cell lysis buffer (catalog no. 9803) was obtained from Cell Signaling Technology. LF3 (catalog no. HY-101486) was acquired from MedChemExpress. PX478 (catalog no. T6961) and KC7F2 (catalog no. T3169) were from Topscience. Matrigel (catalog no. 356237) was obtained from Corning. MG132 (catalog no. 474790) and $CoCl_2$ were from Sigma-Aldrich.

Cell culture

The human colon carcinoma cell line HCT116 was purchased from iCell Bioscience Inc. (catalog no. iCell-h071), maintained in 5A medium, which was supplemented with 10% fetal bovine serum, penicillin (100 IU/ml), and streptomycin (100 mg/ml), and cultured in a humidified atmosphere containing 5% CO_2 at 37°C.

Luciferase reporter construction and assay

The HCT116 luciferase reporter cells for HIF and P53 signaling were created by stably transfecting HCT116 cells with HIF luciferase reporter plasmid (Genomeditech, GM-021020) or p53 luciferase reporter plasmid (GM-021040). PPARγ reporter cells were constructed by stably transfecting the pGL4.20 plasmid, which was inserted 23 copies of PPARγ response elements at the Kpn l and Bgl 2 sites, into Chang liver cells. Transfection was conducted with Lipofectamine 3000 (Invitrogen) per the manufacturer′s protocol. Forty-eight hours after transfection, positive clones were selected by 3 weeks of G418 (500 μg/ml; Sigma-Aldrich) treatment. HCT116 luciferase reporter cells for WNT and STAT-NFκB (*48*) have been described previously. Ten thousand reporter cells were seeded into each well in white 96-well plates and incubated with or without chemicals at the indicated concentrations. After 24 hours, each well was given luciferase assay reagent (Promega) and a SpectraMaxL microplate reader was used to determine the fluorescence value.

Cell viability assay

Three thousand cells were plated into each well of 96-well plates. After overnight culture, the cells were treated with either vehicle or chemical at indicated concentrations. After 72 hours, cell viability was measured with a SpectraMaxi3 microplate reader at a 490-nm emission wavelength by MTT [3-(4,5-dimethylthiazol-2-yl)-2,5-diphenyltetrazolium bromide] assay.

Real-time PCR measurement

Total RNA in HCT116 cells was extracted using RNAisoPlus (TaKaRa, catalog no. 9109), and complementary DNA (cDNA) was generated using a PrimeScript RT reagent kit (Roche). Each cDNA sample was amplified in a StepOne Plus RT-PCR machine (Applied Biosystems) using SYBR Green dye (Roche, catalog no. RR037A). The primer sequences were as follows: Bnip3, 5′-CAGGGCTCCTGGGTAGAACT-3′ (forward) and 5′-CTCCGTCCAGACTCATGCTG-3′ (reverse); Pgk1, 5′-GAACAAGGTTAAAGCCGAGCC-3′ (forward) and 5′-GTGGCAGATTGACTCCTACCA-3′ (reverse); Cyclin D1, 5′-CCATCCAGTGGAGGTTTGTC-3′ (forward) and 5′-AGCGTATCGTAGGAGTGGGA-3′ (reverse); Axin2, 5′-ACTGCCCACACGATAAGGAG-3′ (forward) and 5′-CTGGCTATGTCTTTGGACCA-3′ (reverse); and β-actin, 5′-AGAGCTACGAGCTGCCTGAC-3′ (forward) and 5′-AGCACTGTGTTGGCGTACAG-3′ (reverse). The individual experiments were repeated for three times, and each sample had three technical replicates.

Western blotting

Total protein was extracted using cell lysis buffer (Cell Signaling Technology, catalog no. 9803) with inhibitors cocktail of phosphatase (Roche, catalog no. 4906837001) and protease (Roche, catalog no. 04693132001). Twenty micrograms per lane of total protein was separated by SDS–polyacrylamide gel electrophoresis and then transferred onto nitrocellulose membranes (GE Healthcare, catalog no. 10600034). The membranes were further blocked with 5% nonfat milk in 1× tris buffered saline with tween-20 (TBST) (0.05% Tween-20) for 1 to 1.5 hours at room temperature. Then, the primary antibodies were added to the membranes and incubated overnight at 4°C, followed by a 2-hour incubation with the corresponding horseradish peroxide–conjugated secondary antibodies at room temperature on the second day. After applying the ECL chemiluminescence reagent (Nanjing KeyGen Biotech, catalog no. KGP1121,) the bands were visualized with a Tanon 5200 imaging system. The quantification of the bands was performed by ImageJ software.

3D cell culture model

A 3D cell culture was performed following the previously reported protocol (*58*). Briefly, cells were seeded in a 24-well plate (80,000 per well) and incubated with **3g** or vehicle for 8 days. Spheroids were observed every 2 days, and the diameters of spheroids were quantified with ImageJ. Cells were lysed at the end of the experiments, and the BCA Protein Assay Kit (Solarbio) was used to determine the protein concentrations.

Statistical analysis

Statistical analysis was performed in GraphPad Prism 7.0. Results were presented as means ± SD. Statistical significance was calculated by one-way or two-way analysis of variance (ANOVA). $^*P < 0.05$ was considered statistically substantial.

Supplementary Materials

This PDF file includes:

Figs. S1 to S16
Tables S1 to S5
Spectral Data
References

Other Supplementary Material for this manuscript includes the following:

Data files S1 and S2

REFERENCES AND NOTES

1. X. Wu, C. Zhu, Radical-mediated remote functional group migration. *Acc. Chem. Res.* **53**, 1620–1636 (2020).
2. T. M. Monos, R. C. McAtee, C. R. J. Stephenson, Arylsulfonylacetamides as bifunctional reagents for alkene aminoarylation. *Science* **361**, 1369–1373 (2018).
3. S. R. Chemler, Copper′s contribution to amination catalysis. *Science* **341**, 624–626 (2013).
4. C. R. Pitts, B. Ling, J. A. Snyder, A. E. Bragg, T. Lectka, Aminofluorination of cyclopropanes: A multifold approach through a common, catalytically generated intermediate. *J. Am. Chem. Soc.* **138**, 6598–6609 (2016).
5. M. A. A. Walczak, T. Krainz, P. Wipf, Ring-strain-enabled reaction discovery: New heterocycles from bicyclo[1.1.0]butanes. *Acc. Chem. Res.* **48**, 1149–1158 (2015).
6. J. Kanazawa, K. Maeda, M. Uchiyama, Radical multicomponent carboamination of [1.1.1]propellane. *J. Am. Chem. Soc.* **139**, 17791–17794 (2017).
7. R. Gianatassio, J. M. Lopchuk, J. Wang, C.-M. Pan, L. R. Malins, L. Prieto, T. A. Brandt, M. R. Collins, G. M. Gallego, N. W. Sach, J. E. Spangler, H. Zhu, J. Zhu, P. S. Baran, Organic chemistry. Strain-release amination. *Science* **351**, 241–246 (2016).
8. K. Jana, A. Bhunia, A. Studer, Radical 1,3-difunctionalization of allylboronic esters with concomitant 1,2-boron shift. *Chem* **6**, 512–522 (2020).
9. Q. Zhang, M. F. Chiou, C. Ye, X. Yuan, Y. Li, H. Bao, Radical 1,2,3-tricarbofunctionalization of α-vinyl-β-ketoesters enabled by a carbon shift from an all-carbon quaternary center. *Chem. Sci.* **13**, 6836–6841 (2022).
10. Z. Wu, X. Xu, J. Wang, G. Dong, Carbonyl 1,2-transposition through triflate-mediated α-amination. *Science* **374**, 734–740 (2021).
11. S. Chowdhury, K. N. Owens, R. J. Herr, Q. Jiang, X. Chen, G. Johnson, V. E. Groppi, D. W. Raible, E. W. Rubel, J. A. Simon, Phenotypic optimization of urea-thiophene carboxamides to yield potent, well tolerated, and orally active protective agents against aminoglycoside-induced hearing loss. *J. Med. Chem.* **61**, 84–97 (2018).

12. H. Lu, T.-Y. Yu, P.-F. Xu, H. Wei, Selective decarbonylation via transition-metal-catalyzed carbon–carbon bond cleavage. *Chem. Rev.* **121**, 365–411 (2021).
13. C. Jiang, H. Lu, W.-H. Xu, J. Wu, T.-Y. Yu, P.-F. Xu, H. Wei, Ni-catalyzed 1,2-acyl migration reactions triggered by C–C bond activation of ketones. *ACS Catal.* **10**, 1947–1953 (2019).
14. G. Fumagalli, S. Stanton, J. F. Bower, Recent methodologies that exploit C–C single-bond cleavage of strained ring systems by transition metal complexes. *Chem. Rev.* **117**, 9404–9432 (2017).
15. P. H. Chen, B. A. Billett, T. Tsukamoto, G. Dong, "Cut and sew" transformations via transition-metal-catalyzed carbon-carbon bond activation. *ACS Catal.* **7**, 1340–1360 (2017).
16. L. Souillart, N. Cramer, Catalytic C–C bond activations via oxidative addition to transition metals. *Chem. Rev.* **115**, 9410–9464 (2015).
17. W. Liu, C. -J. Li, Recent synthetic applications of catalyst-free photochemistry. *Synlett* **28**, 2714–2754 (2017).
18. X. Y. Yu, J. R. Chen, W. J. Xiao, Visible light-driven radical-mediated C-C bond cleavage/functionalization in organic synthesis. *Chem. Rev.* **121**, 506–561 (2021).
19. K. N. Houk, The photochemistry and spectroscopy of β,γ-unsaturated carbonyl compounds. *Chem. Rev.* **76**, 1–74 (1976).
20. S. Wilsey, M. J. Bearpark, F. Bernardi, M. Olivucci, M. A. Robb, Mechanism of the oxadi-π-methane and [1,3]-acyl sigmatropic rearrangements of β,γ-enones: A theoretical study. *J. Am. Chem. Soc.* **118**, 176–184 (1996).
21. H. Suginome, M. Takemura, N. Shimoyama, K. Orito, Photoinduced molecular transformations. Part 126. Photo-double ring contraction of 4a-homo-5α-cholest-3-en-1-one, a steroidal β,γ-unsaturated cyclic ketone, involving photochemical 1,3-acyl migration. *J. Chem. Soc. Perkin Trans.* **1**, 2721–2723 (1991).
22. C. K. Prier, D. A. Rankic, D. W. MacMillan, Visible light photoredox catalysis with transition metal complexes: Applications in organic synthesis. *Chem. Rev.* **113**, 5322–5363 (2013).
23. A. B. Beeler, Introduction: Photochemistry in organic synthesis. *Chem. Rev.* **116**, 9629–9630 (2016).
24. X. Wu, Z. Ma, T. Feng, C. Zhu, Radical-mediated rearrangements: Past, present, and future. *Chem. Soc. Rev.* **50**, 11577–11613 (2021).
25. Z. M. Chen, X. M. Zhang, Y. Q. Tu, Radical aryl migration reactions and synthetic applications. *Chem. Soc. Rev.* **44**, 5220–5245 (2015).
26. X. Tang, A. Studer, Alkene 1,2-difunctionalization by radical alkenyl migration. *Angew. Chem. Int. Ed.* **57**, 814–817 (2018).
27. F. Ghorbani, S. A. Harry, J. N. Capilato, C. R. Pitts, J. Joram, G. N. Peters, J. D. Tovar, I. Smajlagic, M. A. Siegler, T. Dudding, T. Lectka, Carbonyl-directed aliphatic fluorination: A special type of hydrogen atom transfer beats out Norrish II. *J. Am. Chem. Soc.* **142**, 14710–14724 (2020).
28. H. Zhang, Y. Song, J. Zhao, J. Zhang, Q. Zhang, Regioselective radical aminofluorination of styrenes. *Angew. Chem. Int. Ed.* **53**, 11079–11083 (2014).
29. J. Gong, P. L. Fuchs, Alkynylation of C—H bonds via reaction with acetylenic triflones1. *J. Am. Chem. Soc.* **118**, 4486–4487 (1996).
30. Q. Michaudel, D. Thevenet, P. S. Baran, Intermolecular ritter-type C–H amination of unactivated sp3 carbons. *J. Am. Chem. Soc.* **134**, 2547–2550 (2012).
31. G. L. Wang, B. H. Jiang, E. A. Rue, G. L. Semenza, Hypoxia-inducible factor 1 is a basic-helix-loop-helix-PAS heterodimer regulated by cellular O_2 tension. *Proc. Natl. Acad. Sci. U.S.A.* **92**, 5510–5514 (1995).
32. P. Jaakkola, D. R. Mole, Y. M. Tian, M. I. Wilson, J. Gielbert, S. J. Gaskell, A. von Kriegsheim, H. F. Hebestreit, M. Mukherji, C. J. Schofield, P. H. Maxwell, C. W. Pugh, P. J. Ratcliffe, Targeting of HIF-α to the von Hippel-Lindau ubiquitylation complex by O_2-regulated prolyl hydroxylation. *Science* **292**, 468–472 (2001).
33. W. G. Kaelin Jr., P. J. Ratcliffe, Oxygen sensing by metazoans: The central role of the HIF hydroxylase pathway. *Mol. Cell* **30**, 393–402 (2008).
34. W. Goessling, T. E. North, S. Loewer, A. M. Lord, S. Lee, C. L. Stoick-Cooper, G. Weidinger, M. Puder, G. Q. Daley, R. T. Moon, L. I. Zon, Genetic interaction of PGE2 and Wnt signaling regulates developmental specification of stem cells and regeneration. *Cell* **136**, 1136–1147 (2009).
35. N. Krishnamurthy, R. Kurzrock, Targeting the Wnt/β-catenin pathway in cancer: Update on effectors and inhibitors. *Cancer Treat. Rev.* **62**, 50–60 (2018).
36. R. H. Giles, M. P. Lolkema, C. M. Snijckers, M. Belderbos, P. van der Groep, D. A. Mans, M. van Beest, M. van Noort, R. Goldschmeding, P. J. van Diest, H. Clevers, E. E. Voest, Interplay between VHL/HIF1α and Wnt/β-catenin pathways during colorectal tumorigenesis. *Oncogene* **25**, 3065–3070 (2006).
37. J. H. Lim, Y. S. Chun, J. W. Park, Hypoxia-inducible factor-1α obstructs a Wnt signaling pathway by inhibiting the hARD1-mediated activation of β-catenin. *Cancer Res.* **68**, 5177–5184 (2008).
38. A. Kaidi, A. C. Williams, C. Paraskeva, Interaction between β-catenin and HIF-1 promotes cellular adaptation to hypoxia. *Nat. Cell Biol.* **9**, 210–217 (2007).
39. Z. Tang, B. Kang, C. Li, T. Chen, Z. Zhang, GEPIA2: An enhanced web server for large-scale expression profiling and interactive analysis. *Nucleic Acids Res.* **47**, W556–W560 (2019).
40. W. H. Urry, D. J. Trecker, Photochemical reactions of 1,2-diketones. *J. Am. Chem. Soc.* **84**, 118–120 (1962).
41. M. Meanwell, J. Lehmann, M. Eichenberger, R. E. Martin, R. Britton, Synthesis of acyl fluorides via photocatalytic fluorination of aldehydic C-H bonds. *Chem. Commun.* **54**, 9985–9988 (2018).
42. W. G. McGimpsey, J. C. Scaiano, A two-photon study of the "reluctant" Norrish type I reaction of benzil. *J. Am. Chem. Soc.* **109**, 2179–2181 (1987).
43. J. Morin, A. B. Sparks, V. Korinek, N. Barker, H. Clevers, B. Vogelstein, K. W. Kinzler, Activation of β-catenin-Tcf signaling in colon cancer by mutations in β-catenin or APC. *Science* **275**, 1787–1790 (1997).
44. P. Hou, F. Chen, H. Yong, T. Lin, J. Li, Y. Pan, T. Jiang, M. Li, Y. Chen, J. Song, J. Zheng, J. Bai, PTBP3 contributes to colorectal cancer growth and metastasis via translational activation of HIF-1α. *J. Exp. Clin. Cancer Res.* **38**, 301 (2019).
45. J. Zhang, J. Cao, Q. Weng, R. Wu, Y. Yan, H. Jing, H. Zhu, Q. He, B. Yang, Suppression of hypoxia-inducible factor 1α (HIF-1α) by tirapazamine is dependent on eIF2α phosphorylation rather than the mTORC1/4E-BP1 pathway. *PLOS ONE* **5**, e13910 (2010).
46. H. S. Ban, B. K. Kim, H. Lee, H. M. Kim, D. Harmalkar, M. Nam, S. K. Park, K. Lee, J. T. Park, I. Kim, K. Lee, G. S. Hwang, M. Won, The novel hypoxia-inducible factor-1α inhibitor IDF-11774 regulates cancer metabolism, thereby suppressing tumor growth. *Cell Death Dis.* **8**, e2843 (2017).
47. Y. Yan, Y. Zhang, M. Li, Y. Zhang, X. Zhang, X. Zhang, Y. Xu, W. Wei, J. Wang, X. Xu, Q. Song, C. Zhao, C644-0303, a small-molecule inhibitor of the Wnt/β-catenin pathway, suppresses colorectal cancer growth. *Cancer Sci.* **112**, 4722–4735 (2021).
48. M. Li, Y. Yan, X. Zhang, Y. Zhang, X. Xu, L. Zhang, L. Lu, J. Wang, Y. Zhang, Q. Song, C. Zhao, Scaffold compound L971 exhibits anti-inflammatory activities through inhibition of JAK/STAT and NFκB signalling pathways. *J. Cell. Mol. Med.* **25**, 6333–6347 (2021).
49. T. Narita, S. Yin, C. F. Gelin, C. S. Moreno, M. Yepes, K. C. Nicolaou, E. G. Van Meir, Identification of a novel small molecule HIF-1α translation inhibitor. *Clin. Cancer Res.* **15**, 6128–6136 (2009).
50. A. Daina, O. Michielin, V. Zoete, SwissADME: A free web tool to evaluate pharmacokinetics, drug-likeness and medicinal chemistry friendliness of small molecules. *Sci. Rep.* **7**, 42717 (2017).
51. J. P. Piret, D. Mottet, M. Raes, C. Michiels, $CoCl_2$, a chemical inducer of hypoxia-inducible factor-1, and hypoxia reduce apoptotic cell death in hepatoma cell line HepG2. *Ann. N. Y. Acad. Sci.* **973**, 443–447 (2002).
52. R. Archid, W. Solass, C. Tempfer, A. Konigsrainer, M. Adolph, M. A. Reymond, R. B. Wilson, Cachexia anorexia syndrome and associated metabolic dysfunction in peritoneal metastasis. *Int. J. Mol. Sci.* **20**, 5444 (2019).
53. J. R. Graff, B. W. Konicek, J. H. Carter, E. G. Marcusson, Targeting the eukaryotic translation initiation factor 4E for cancer therapy. *Cancer Res.* **68**, 631–634 (2008).
54. C. Qi, J. Zhang, X. Chen, J. Wan, J. Wang, P. Zhang, Y. Liu, Hypoxia stimulates neural stem cell proliferation by increasing HIF1α expression and activating Wnt/β-catenin signaling. *Cell. Mol. Biol. (Noisy-le-Grand)* **63**, 12–19 (2017).
55. N. E. Ryu, S. H. Lee, H. Park, Spheroid culture system methods and applications for mesenchymal stem cells. *Cell* **8**, 1620 (2019).
56. G. L. Semenza, Hypoxia-inducible factors: Mediators of cancer progression and targets for cancer therapy. *Trends Pharmacol. Sci.* **33**, 207–214 (2012).
57. S. L. Schreiber, Target-oriented and diversity-oriented organic synthesis in drug discovery. *Science* **287**, 1964–1969 (2000).
58. G. Y. Lee, P. A. Kenny, E. H. Lee, M. J. Bissell, Three-dimensional culture models of normal and malignant breast epithelial cells. *Nat. Methods* **4**, 359–365 (2007).
59. P. A. Evans, S. Oliver, J. Chae, Rhodium-catalyzed allylic substitution with an acyl anion equivalent: Stereospecific construction of acyclic quaternary carbon stereogenic centers. *J. Am. Chem. Soc.* **134**, 19314–19317 (2012).
60. W. Li, P. Jia, B. Han, D. Li, W. Yu, Cobalt-catalyzed aerobic oxidative cyclization of β,γ-unsaturated oximes. *Tetrahedron* **69**, 3274–3280 (2013).
61. R. Liu, O. Gutierrez, D. J. Tantillo, J. Aube, Stereocontrol in a combined allylic azide rearrangement and intramolecular Schmidt reaction. *J. Am. Chem. Soc.* **134**, 6528–6531 (2012).
62. D. L. J. Clive, C. G. Russell, S. C. Suri, Alpha. Vinylation of ketones. A general method using (phenylseleno)acetaldehyde. *J. Org. Chem.* **47**, 1632–1641 (1982).
63. R.-H. Liu, D. Wei, B. Han, W. Yu, Copper-catalyzed oxidative oxyamination/diamination of internal alkenes of unsaturated oximes with simple amines. *ACS Catal.* **6**, 6525–6530 (2016).
64. R. Matovic, A. Ivkovic, M. Manojlovic, Z. Tokic-Vujosevic, R. N. Saicic, Ring closing metathesis/fragmentation route to (Z)-configured medium ring cycloalkenes. Total synthesis of (±)-periplanone C. *J. Org. Chem.* **71**, 9411–9419 (2006).
65. F. A. Davis, H. Zhang, S. H. Lee, Masked oxo sulfinimines (*N*-sulfinyl imines) in the asymmetric synthesis of proline and pipecolic acid derivatives. *Org. Lett.* **3**, 759–762 (2001).

Acknowledgments: We thank Shandong Lead High Biotechnology Co. Ltd. for providing laboratories for synthesizing different β,γ-unsaturated ketones. We also thank H. Sui and X. Li from Shandong University Core Facilities for Life and Environmental Sciences for their help with the NMR. **Funding:** This work was funded by the National Program for Support of Top-notch Young Professionals, the Fund of Taishan Scholar Project, the Shandong Provincial Natural Science Foundation for Distinguished Young Scholars (JQ201722), the Qingdao Science and Technology Benefit People Demonstration Guide Special Project (20-3-4-20-nsh), the Joint Fund of Shandong Natural Science Foundation (ZR2021LSW013), the Postdoctoral Science Foundation of China (2020 M672077), the Natural Science Foundation for Youths of Shandong Province of China (ZR2022QB090), the Postdoctoral Applied Research Project of Qingdao (62450070311120), the Fundamental Research Funds of Shandong University (2020GN033), the Shandong Province Major Scientific and Technological Innovation Project (2020CXGC010503), the Shandong Provincial Key Laboratory Platform Project (2021ZDSYS11), and the National Natural Science Foundation of China Major Project (81991525). **Author contributions:** R.L., J.Y., and D.S. conceived and designed the project. R.L., Y.T., J.W., R.Y., S.L., and L.Y. performed the experiments. R.L., Z.W., S.L., L.Y., X.L., and C.Z. isolated all products and discussed the results. R.L., D.S., and C.Z. wrote and revised the manuscript. R.L., R.Y., J.W., and L.Y. prepared and wrote the Supplementary Materials and contributed other related materials. **Competing interests:** D.S., R.L., and Y.T. are inventors on a patent application related to this work filed by Shandong Lead High Biotechnology Co. Ltd. (no. CN202110321245.4, filed on 25 March 2021). D.S., R.L., Y.T., X.L., and C.Z. are inventors on a patent application related to this work filed by Shandong Lead High Biotechnology Co. Ltd. (no. CN202110987570.4, filed on 16 November 2021). The authors declare no other competing interests. **Data and materials availability:** All data needed to evaluate the conclusions in the paper are present in the paper and/or the Supplementary Materials.

Submitted 11 May 2022
Accepted 3 November 2022
Published 9 December 2022
10.1126/sciadv.abq8596